Photochemical & Photobiological Sciences (2026) 25:1951–1969
https://doi.org/10.1007/s43630-026-00971-4

RESEARCH

Recent increases in solar UV radiation across Europe: a 40-location study to identify trend boundaries

Alois W. Schmalwieser[1] · Sebastian Lorenz[2] · Dariia Klyshkina[1] · Barbara Klotz[3] · Michael Schwarzmann[3] · Stana Simic[4] · Alexander Mangold[5] · Natacha Pezzetti[5] · Kamil Láska[6] · Marie Novotná[6] · Martin Stráník[7] · Brian Køster[8] · Margit Aun[9] · Kaisa Lakkala[10,11] · Frederique Auriol[12] · Eric Bourrianne[12] · Romain De Filippi[12] · Nicolas Henriot[12] · Fanny Minvielle[12] · Jörg Trentmann[13] · Daniela Weiskopf[2] · Alkiviadis Bais[14] · Katerina Garane[14] · Dénes Fekete[15] · Annachiara Bellini[16] · Alcide Giorgio di Sarra[17] · Henri Diémoz[16] · Luca Fibbi[18,19] · Francesca Frasca[20] · Daniele Grifoni[18,19] · Daniela Meloni[17] · Anna Maria Siani[20] · Peter den Outer[21] · Jos van Geffen[22] · Edith van Putten[21] · Bjørn Johnsen[23] · Tove Svendby[24] · Agnieszka Czerwińska[25] · Janusz Krzyścin[25] · Natalia Chubarova[26] · Slavica Malinović-Milićević[27,28] · Zoltan Nađ[29] · Zorica Podrascanin[29] · Anna Pribullova[30] · Juana Arolo Pacheco[31] · Ana Díaz Rodriguez[31] · Carmen González[32] · José Manuel Vilaplana[32] · Julian Gröbner[33] · Gregor Hülsen[33] · Michael Higlett[34] · Andrey Lyachev[34] · Rebecca Rendell[34] · Andrew R. D. Smedley[35] · Ann Webb[35]

Received: 28 May 2026 / Accepted: 26 July 2026 / Published online: 12 August 2026
© The Author(s) 2026

Abstract
Significant trends of ultraviolet radiation (UVR) have been reported at limited European sites due to changing atmospheric conditions, such as cloudiness. Whether these findings are applicable to larger areas or even the entire continent remains unclear. In a unique comparison, we analyzed measurements of erythemally weighted daily ambient radiant exposure from 40 European locations, covering the period from 2013 to 2022. At 26 locations annual means increases statistically significantly with a median of +1.2%/yr. At 38 sites at least monthly means increases with medians between +2%/yr and +4%/yr. Increases were seen in satellite products of UVR, global solar radiation, and sunshine duration, too. Analysis at six stations, with data extending back to the mid-1990s, indicates that the period of statistically significant increases generally began between 2010 and 2013. Comparison of UVR data from 40 stations with a high-resolution global solar radiation trend map reveals complementary patterns, highlighting widespread but not uniform UVR changes across Europe. This combination enables figuring out the regional extent of trends. Thus, ground-based UVR measurements remain essential for quantifying changes, highlighting the need for continued monitoring with sufficiently dense measurement networks. This is also essential for understanding and mitigating the impacts of changing UVR on human health, particularly by assessing its potential for increased UVR-related skin cancer incidence and development of preventive measures. Moreover, detailed regional UVR data is essential for achieving the UN's Sustainable Development Goals, specifically in human health, sustainable cities, climate action, and environmental conservation.

Keywords Solar ultraviolet radiation · Erythemally effective ultraviolet radiation · Trend analysis · Sunshine duration · Global solar radiation · Human health · Climate change · UV radiation exposure

1 Introduction

The amount of solar ultraviolet radiation (UVR) reaching the Earth's surface depends on several astronomical and atmospheric factors. The distance between the Earth and the Sun follows a cyclical change throughout the year and the Earth's axis is inclined to its plane of rotation around the sun. The latter, together with geographical position on the Earth determines the solar elevation and the duration of daylight at any point and time. Solar elevation and altitude above sea level define the length of the pathway of solar radiation through the atmosphere, and with that the amount

Extended author information available on the last page of the article

of absorption and scattering in the atmosphere. The ozone layer in the stratosphere absorbs the UV-C radiation completely, partially absorbs UV-B radiation and leaves UV-A radiation almost unaffected. Atmospheric aerosols attenuate UVR to some extent with reduction (absorption and enhanced scattering) dependent on the type of aerosols and the wavelength (greater reduction at shorter wavelengths) [1]. Especially in urban regions with poor air quality, reduction by aerosols can be noticeable [2]. The greatest transient effect on UVR comes from cloudiness. While heavy rain clouds can reduce UVR to almost zero, broken clouds can temporarily increase UVR compared to clear sky conditions by modifying the scattering of the solar beam [3]. At the ground, the surface albedo (reflection from the ground) can enhance UVR noticeably in regions with ice and snow, but only minimally in the presence of most other natural surfaces [4]. The effect of albedo can be enhanced under cloudy skies due to backscattering of reflected radiation [5]. Understanding the underlying mechanisms controlling UVR at the surface is crucial for assessing its impact on the biosphere.

Solar UVR is vital for most life forms as it regulates growth of plants, initiates photosynthesis of Vitamin D in many kinds of vertebrates or is used for vision, orientation and foraging for food [6]. Life has adapted to local levels of UVR over evolutionary time scales and developed a range of adaptive mechanisms to counteract seasonal variations in UVR or longer-term migration patterns (e.g. changes in skin thickness and pigmentation) [7, 8]. Nonetheless, overexposure may still occur but can be mitigated to some extent by intrinsic mechanisms like UVR initiated photo-repair [9]. In the case of humans, it was recognized early that enhanced UVR exposure (relative to evolutionarily developed skin type) is detrimental. In addition to reversible short-term injuries from overexposure, like sunburn or inflammations of the eye, there is damage from long-term exposure and repeated overexposure [10].

UVR is the primary environmental risk factor for both melanoma and keratinocyte skin cancers [11]. Individual risk varies due to genetics and skin type, but cumulative lifetime UVR exposure and history of sunburns remain the primary drivers. Populations with lighter skin pigmentation, particularly those of European ancestry (including populations in the United States and Australia), exhibit the highest incidence rates of skin cancer, where permanent (migration) or intermittent (holiday) UVR exposure exceeds that of their natural ancestral environment. In Europe, approximately 150,000 new cases of melanoma are diagnosed annually [12], accounting for nearly half of all cases worldwide and more than 25,000 deaths in Europe are attributed to melanoma each year. Significantly more common than melanoma are keratinocyte skin cancers, including squamous cell carcinoma and basal cell carcinoma; however, they are not consistently registered across countries, leading to underestimation of their true incidence [13–15].

Several studies have reported increasing UV irradiance in Europe in recent years [16–22], while other studies report no such trends [23, 24]. Due to different periods of study, distinct geographical location and calculation methods, it is challenging to attribute widespread trends to a specific period or a specific region. Therefore, this study aims to investigate where changes in UVR have occurred and how widespread these are across Europe through the largest comparative analysis of ground-based UVR data to date. To incorporate high quality data from as many stations as possible, it is essential to select a time period that is not too long, because the number of UVR monitoring stations has grown over time [25], while quality assurance and quality control procedures have also gradually developed through time [26]. On the other hand, the period must not be too short, because the impact of interannual variability should be minimized to enable statistical significance. Therefore, we selected the 10-year period from 2013 to 2022, which was previously successfully used to demonstrate the influence of decreasing cloud cover and related increasing global solar radiation on global temperature [27].

In addition to UVR data, we considered UVR related parameters including total ozone column, sunshine duration (primarily influenced by cloudiness) and global solar radiation (primarily influenced by cloudiness and aerosol optical depth). For global solar radiation it was recently shown [21] that annual differences in UVR generally align with annual differences in global solar radiation. Furthermore, good agreement has been found between satellite-based high resolution spatial data of global solar radiation and corresponding ground-based global solar radiation measurements [28]. By introducing such additional data, this study aims to provide new insights into the spatial patterns of UVR changes across Europe by linking highly resolved spatial trends in global solar radiation from satellites with trends in ground-based UVR.

2 Materials and methods

2.1 Ground-based data

2.1.1 Ground-based UV radiation measurements

Forty observatories from across Europe (35°N to 67°N, 9°W to 38°E) provided data of erythemally weighted daily radiant exposure H_{GB} (where the subscript "GB" refers to ground-based data) measured with broadband UV radiometers, filter radiometers or spectroradiometers. Measurements

came from devices with a horizontally oriented receiving surface and a field of view of 180°. Further requirements were that measurements should be taken throughout daylight hours and every day, covering at least the period from 1.1.2013 to 31.12.2022. Additionally, the measuring devices were maintained according to well defined QA/QC procedures over the whole period (for details see references in Table 1). Participating observatories are listed in Table 1 and depicted in Fig. 1.

For erythemal weighting, the action spectrum for human erythema according to ISO/CIE [46] was used. This action spectrum gives lower weight to longer wavelengths by up to a factor of 1/10,000 and therefore erythemally weighted radiant exposure is lower than unweighted radiant exposure over the same wavelength range (280–400 nm). In other words, the erythemal weighed radiant exposure quantifies intensity of the solar radiation causing erythema on the skin. H_{GB} is expressed herein in units of J_{ery}/m^2, where the subscript "ery" is used to indicate that erythemal weighting

Table 1 List of stations, geographical coordinates, used device and a reference for more details

No.	Country	Station	Latitude[°]	Longi-tude [°]	Altitude [m asl]	Device	References
1	AUT	Dornbirn	47.43 N	9.73 E	407	SL 501	[29]
2		Sonnblick	47.05 N	12.96 E	3106	Bentham DM150	[5]
3		Vienna	48.26 N	16.43 E	160	SL 501	[30]
4	BEL	Uccle	50.80 N	4.35 E	100	Brewer MK III, MK II	[15]
5	CZE	Brno-Kotlářská	49.20 N	16.60 E	257	SL 501	--
6		Hradec Králové	50.18 N	15.84 E	278	SL 501	[18]
7		Košetice	49.57 N	15.08 E	534	SL 501	[31]
8	EST	Tartu-Tõravere	58.26 N	26.46 E	70	UVS-E-T	[25]
9	FIN	Sodankylä	67.37 N	26.63 E	179	Brewer MK II	[32]
10	FRA	Lille, Villeneuve d'Ascq, AtOLL	50.61 N	3.14 E	70	Bentham DTMc300	[33]
11		Obs. de Haute-Provence, OHP	43.94 N	5.71 E	650	Bentham DTMc300	[34]
12	GER	Dortmund	51.5 N	7.50 E	130	Bentham DTMc300	[21]
13	GRE	Thessaloniki	40.64 N	22.97 E	80	YES UVB-1	[35]
14	HUN	Budapest	47.43 N	19.18 E	139	SL 501	[25]
15	ITA	Aosta	45.74 N	7.36 E	570	Bentham DTMc300	[20]
16		Lampedusa	35.52 N	12.63 E	45	Brewer MK III	[36]
17		Rome	41.90 N	12.50 E	75	Brewer MK IV	[20]
18		Sesto Fiorentino/Florence	43.82 N	11.20 E	50	SL 501	[25]
19	NDL	Bilthoven	52.12 N	5.19 E	12	DILOR XY, Brewer MK III	[37]
20	NOR	Bergen	60.38 N	5.33 E	40	GUV 541	[38]
21		Landvik	58.33 N	8.52 E	10	GUV 541	[38]
22		Trondheim	63.42 N	10.40 E	65	GUV 541	[38]
23	POL	Belsk	51.84 N	20.79 E	180	SL 501, UV-AE-T	[39]
24	RUS	Moscow	55.71 N	37.52 E	*192*	UVB-1, UVS-E-T	[40]
25	SER	Novi Sad	45.33 N	19.85 E	84	YES UVB- 1	[41]
26	SVK	Poprad-Ganovce	49.03 N	20.32 E	706	SL 501	[25]
27	ESP	A Coruna	43.37 N	8.42 W	57	UVS-E-T	[25]
28		Badajoz	38.89 N	7.01 W	175	YES UVB-1	[25]
29		Barcelona	41.39 N	2.20 E	26	YES UVB-1	[25]
30		Huelva/El Arenosillo	37.10 N	6.73 W	41	YES UVB-1	[42]
31		Madrid	40.45 N	3.72 W	664	YES UVB-1	[25]
32		Malaga	36.72 N	4.48 W	60	YES UVB-1	[25]
33		Valencia	39.49 N	0.47 W	56	YES UVB-1	[25]
34	CHE	Davos	46.80 N	9.83 E	1610	SL 501, UVS-E-T, UVB-1	[25]
35	GBR	Camborne	50.22 N	5.33 W	81	SL 501	[43]
36		Chilton	51.58 N	1.32 W	123	SL 501	[44]
37		Glasgow	55.86 N	4.34 W	9	SL 501	[43]
38		Lerwick	60.14 N	1.19 W	80	SL 501	[43]
39		Manchester	53.47 N	2.23 W	76	Brewer Mk III	[45]
40		Reading	51.44 N	0.94 W	66	Bentham DM150	[45]

Broadband meters: SolarLight SL501, Yankee Environmental Systems YES UVB-1, Kipp&Zonen UVS-E-T and UV-AE-T. Multichannel instrument: Biospherical instruments GUV-541. Spectroradiometers: SCI-TEC/Kipp&Zonen Brewer Mk II, MK III and MK IV, Bentham Instruments DTM150, DTMc300, Dilor DILOR-XY

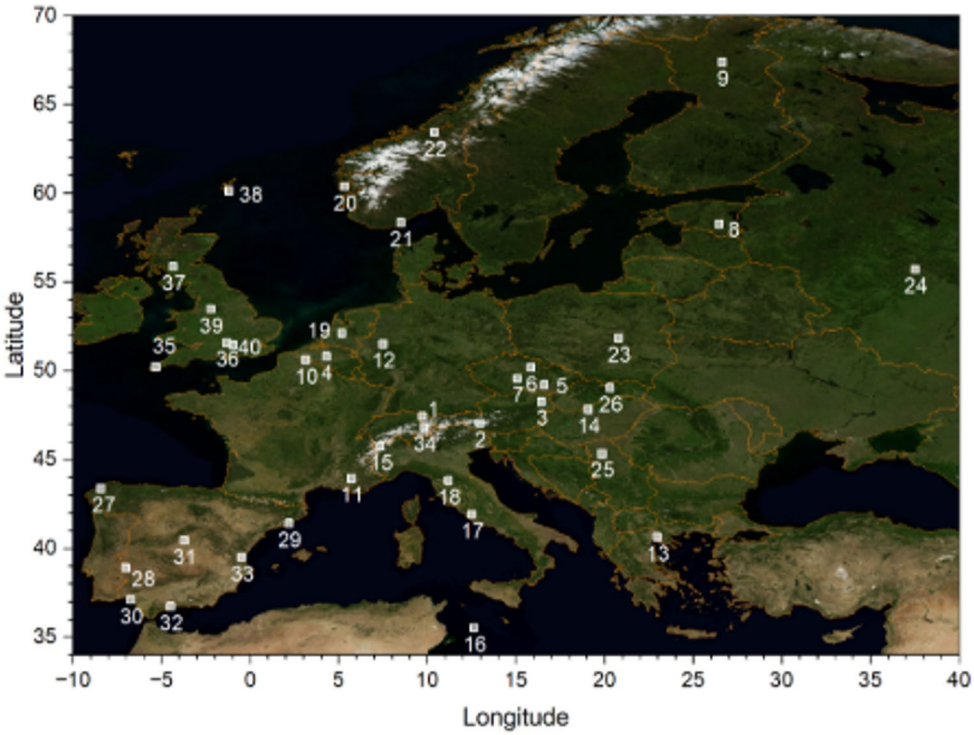


Fig. 1 Stations contributing data in this study on the Blue Marble Map, July 2004 from NASA Earth Observatory [47]

has been applied. H_{GB} can also be expressed in units of the Standard Erythema Dose (SED), where 1 SED = 100 J_{ery}/m^2 [46].

2.1.2 Mean values and data gaps of ground-based measurements

The duty cycle of ground-based measurements is generally lower than 100% for reasons such as device maintenance, calibration or accidental shutdowns from power loss or instrument malfunctions. Therefore, temporal gaps occur in every data set. Depending on date and duration, data gaps may influence monthly and annual mean values to different extents. A priori, only complete daily integrals were accepted for the calculation of monthly mean values and no more than five missing days were permitted for a valid monthly mean in any particular year. Annual means were calculated from monthly means. Ten observatories achieved these criteria for all monthly means, while for 25 of the stations, some monthly means were substituted by the median of the corresponding valid monthly means available in the period of 2013 to 2022. For observatories where more advanced and validated data gap handling methods have already been applied in the past, we used the corresponding dataset in this study. These extended methods incorporate e.g. additional local ground-based measurements, such as pyranometer data, to account for weather conditions [38, 48].

2.1.3 Ground-based measurements of sunshine duration

Out of the 40 observatories, 27 could also provide data for sunshine duration SSD_{GB} for the same or a nearby location. Measurements of SSD_{GB} result generally from sunshine duration recorders. The WMO (World Meteorological Organization) defines the sunshine duration as the time during which the direct solar irradiance exceeds 120 W/m² [49]. This corresponds to the irradiance which is needed to burn a trace on the card of the classical Campbell-Stokes recorder. With that it is also possible to calculate sunshine duration from the difference between measurements of total and diffuse global solar radiation, which gives the direct solar irradiance, corrected for solar elevation. Consequently, sunshine duration is a valuable parameter for assessing changes in cloudiness, as it is primarily driven by cloud variability.

2.2 Satellite based data

2.2.1 Daily radiant exposure and total ozone column from the ozone monitoring instrument

Erythemally weighted cloud modified daily radiant exposure H_{OMI} is also available from NASA's Ozone Monitoring Instrument (OMI) onboard the AURA satellite. The instrument provides measurements at overpass around 13:45 local solar time for a 17 × 24 km region. Radiance is measured at several wavelengths in the UV range, once directly from the sun and once backscattered from the atmosphere. From

these measurements, erythemally weighted daily radiant exposure is calculated [50, 51] globally for a 1°x1° grid (and made available within the so-called OMUVBd data set) [50]. Data are available since October 2004 with a duty cycle of around 300 days per year. However, AURA's orbit does not allow full coverage of the whole globe each day so that crescent-like data gaps appear which are broadest at the equator. Due to these gaps, data yield may be reduced depending on location. For the location of Vienna (48°N), for example, around 218 values per year are available. As the gaps appear with fixed periodicity during the year, their influence on monthly and annual means is the same for all years. Therefore, there is no need to fill data gaps by a substitution method. For each participating station, bilinear spatial interpolation from four surrounding grid points was applied to derive the corresponding OMI data. OMI's erythemally weighted daily radiant exposure data has previously been validated for several locations [52–59] and full agreement between H_{OMI} and H_{GB} should not be expected because OMI measurements are taken at noon and extrapolated for the whole day, and are representative for a 1°x1° grid rather than for a single ground-based location.

Total ozone column (TOC) was also received from NASA's OMI. Duty cycle and data yield is the same as for H_{OMI}. TOC was obtained for each location using spatial interpolation from the 1°x1° grid as for H_{GB}.

2.2.2 Satellite based daily radiant exposure from TEMIS

The Thematic Emission Monitoring Integrated Service (TEMIS) UV radiation data services – supported by the European Space Agency (ESA) and hosted by the Royal Netherlands Meteorological Institute (KNMI)—provides the cloud-modified erythemally effective daily radiant exposure (H_{TEMIS}) over large parts of Europe and Africa. H_{TEMIS} results from a parameterisation developed by Allaart et al. [60] using measurements from Brewer spectroradiometers at De Bilt (The Netherlands) and Paramaribo (Suriname). Besides solar zenith angle, the parameterisation uses the ozone column at local solar noon from the operational TEMIS global assimilated ozone field [61], which is obtained from daily satellite observations of total ozone (from ESA's GOME-2 C (Global Ozone Monitoring Experiment) satellite and its predecessors) and the European Centre for Medium-Range Weather Forecasts (ECMWF) analysis and forecast data. In 2017 TEMIS version 2.0 [62] was released with full reprocessing of all data. This version features, among others, new fit-parameters (based on additional measurements from De Bilt and Paramaribo), improvements in modifying UVR in the presence of clouds and spatial resolution increased to 0.25°x0.25°. Cloud modification is based on the Surface Downwelling Shortwave Flux (0.3–4.0 μm), derived from measurements made by EUMETSAT's (European Organisation for the Exploitation of Meteorological Satellites) geostationary Meteosat (Meteorological satellite) Second Generation (MSG) satellites, and corrected for application in the UV wavelength range. MSG takes measurements every 15 min over Europe and Africa and is available from the MSG Cloud Physical Properties (CPP) project. On average, cloud data is available on 362 days per year for locations with latitudes below about 54°, and less for stations at higher latitudes. All MSG measurements falling within a given UVR grid cell of 0.25°x0.25° are used to determine the cloud modification factor for that grid cell. The daily radiant exposure overpass data for a given ground station is the value of the UVR grid cell within which that ground station is located; no interpolation is performed. Previous TEMIS versions up to 1.4 have been validated in the past for several locations [63] as well as the recent version 2.0 [59]. As in the case of OMI, deviations from H_{GB} should be expected, especially in the presence of clouds and snow. Data are available as a grid (0.25°x0.25°) and as overpass for multiple sites back to January 22, 2004, up to the previous day [62].

2.2.3 Global solar radiation and sunshine duration from SARAH records

The Satellite Application facility on climate monitoring (CM SAF) within EUMETSAT provides the so-called SARAH-3 (SurfAce Radiation dAta set-Heliosat, Edition 3) climate data record [64]. This record provides seven homogenous surface solar radiation parameters including global solar radiation (surface irradiance) and sunshine duration from 1983 onwards with a spatial resolution of 0.05° for the coverage of EUMETSAT's series of Meteosat satellites, i.e. Africa, Europe and parts of South America [65]. Global solar radiation data results from the Heliosat-Method, which uses effective cloud albedo taken respectively from cloud top surface reflectivity from the visible channel of the MVIRI (Meteosat Visible and InfraRed Imager) operated on the Meteosat First Generation (MFG) satellites from 1977 to 2006, and from the SEVIRI (Spinning Enhanced Visible and InfraRed Imager), its successor, that has operated on the Meteosat Second Generation (MSG) satellites since 2002 to the present [66]. Monthly sums of sunshine duration are also derived from measurements of MVIRI and SEVIRI. Calculation of the surface global solar radiation uses a clear-sky surface radiative transfer scheme-called SPECMAGIC [67]—inputting the Heliosat-Method output. SARAH-3 data (further called SARAH) cover the period from 1983 to 2020 as the climate data record (CDR) and this is operationally extended as interim climate data record (ICDR, a near-real-time extension of the established Climate Data Record)

to the present with a latency of 5 days. In principle, the transition from CDR to ICDR may introduce discontinuities; however, these are expected to be limited, as the same set of algorithms is applied.

2.2.4 Global solar radiation from CLARA records

The CLARA-A3 (CM SAF cLoud, Albedo and surface RAdiation dataset from AVHRR data - Edition 3) climate data record [68] is based on measurements from the polar-orbiting NOAA—(National Oceanic and Atmospheric Administration) and MetOp (Meteorological Operational Satellite operated by EUMETSAT) satellites by the AVHRR-instruments (Advanced Very High Resolution Receiver) and contains data on cloud coverage and cloud physical properties, the top-of-atmosphere and the surface radiation, as well as the surface albedo. The estimation of the surface radiation is based on a look-up-table approach that relates the solar radiation (reflected to space) to the cloud transmission, which is used to estimate surface irradiance [69]. The global CLARA-A3 surface radiation data (further called CLARA) are available as daily and monthly averages from 1979 to 2020 as CDR and ICDR onwards with a spatial resolution of 0.25° [70].

2.3 Statistical analysis and trend analysis

Trend analysis was done by applying linear regression analysis (least square) on the data. For testing the statistical significance, we performed a two-sided t-test (increase or decrease) assuming a p-value ≤ 0.1 for significance. Trend analysis was done for annual means as well as separately for each calendar month for the period from 2013 to 2022 (hereafter short-term trend). The 10-year period was chosen to balance data quality and quantity while minimizing the impact of interannual variability. Additionally, this period is expected to show a significant increase in UVR in parts of Europe due to decreasing cloud cover, as indicated by existing data [27, 71]. By selecting this period, we can better detect significant changes in UVR, even with a relatively short time frame. For observatories with longer and complete time series, trend analysis was performed for 10-year periods with a 1-year step width, going back in time until statistically significance vanishes. This allows estimation of when significant changes may have started. Correlation analysis and linear regression analysis for other parameters was performed using one-sided t-test with $p = 0.05$.

3 Results

3.1 Trend analysis of ground-based UV radiation measurements

Linear regression analysis for the period from 2013 to 2022 delivers a statistically significant short-term-trend in the annual mean values of H_{GB} for 26 out of 40 locations. For these stations, all trends are positive, ranging from +0.46%/yr to +2.6%/yr (see Table 2). The median significant trend is +1.16%/yr which corresponds to an increase of the mean daily radiant exposure H_{GB} of +17.3 J_{ery}/m^2 per year. This denotes further that the mean H_{GB}, which is currently around 14 SED (all stations over the whole period), increases every 5 to 6 years by 100 J_{ery}/m^2 or by 1 SED. Table 2 provides the increase for each location in $J_{ery}/m^2/yr$. Figure 2 depicts the spatial distribution of trends. Locations with statistically significant trends are indicated by red columns and insignificant trends by grey columns. It can be seen that significant increases in H_{GB} are spread over a large part of Europe, extending from Scandinavia in the North to Thessaloniki, Greece in the Southeast and from the British Isles in the West to eastern Central Europe, including Belsk, Poland, and Poprad-Ganovce, Slovakia. Although Moscow shows a significant increase (see Table 2), the lack of intermediate stations prevents us from confirming the extension of the significant positive trends to this region. The underlying distribution of annual trends in global solar radiation from SARAH (GSR_{SARAH}) in Fig. 2, described in more detail below, exhibits a very similar pattern and suggests that the Central European UVR increase may not extend as far as Moscow. Notably, the Alpine ridge exhibits high spatial variability in trends, forming an alternating pattern that stretches from the Provence region over Switzerland to Austria. The agreement between UVR variability and global solar radiation variability in this region is remarkably high. For Italy and Greece, it can be observed that the positive H_{GB} trends decrease as one move further south or southeast, consistent with changes in GSR_{SARAH}. Similarly, there is a good agreement between the lack of trend in GSR_{SARAH} and H_{GB} in most parts of Spain and on the island of Lampedusa in southern Europe. In the north, the trend is found to weaken in Norway, as described also earlier [38].

A statistically significant trend in the annual mean does not necessarily denote that there is a significant trend in each calendar month. Vice versa there may be significant changes for a few calendar months (e.g. winter) which, when combined with all other months, do not affect the annual mean significantly. Analysis of monthly mean H_{GB} shows that statistically significant increases are found for 38 locations (see Table 2) and most frequently (Fig. 3a, red columns) for January (15/39), February (18/40), June (18/40) and October

Table 2 Statistical analysis of ground-based and satellite-based erythemally weighted daily radiant exposure H (ground-based, OMI, TEMIS), total Ozone column (TOC, from OMI, global solar radiation (GSR, from CLARA and SARAH) and sunshine duration (SSD, ground-based and from SARAH)

No.	Location	H					H		H	
		GB					TEMIS		OMI	
		Mean [J_{ery}/ m²]	k [%/yr]	sig.	k [J_{ery} /m²/yr]	Sig. months	k [%/yr]	Sig.	k [%/yr]	Sig.
1	Dornbirn, AUT	1563	+1.28	*	+20.09	2: V. VI	+1.64	*	+1.22	*
2	Sonnblick, AUT	2095	+0.02		+0.40	3: I. II. X	+2.64	*	+1.26	*
3	Wien, AUT	1477	+0.63	*	+9.30	1: VI	+1.07	*	+0.70	*
4	Uccle, BEL	1345	+1.47	*	+19.72	4: II. III. V. VI	+1.41	*	+0.79	
5	Brno-Kotlářská, CZE	1442	+1.46	*	+20.88	5: I. II. IX. X. XI	+1.18	*	+0.76	*
6	Hradec Králové, CZE	1437	+0.73		+10.45	3: I. II. X	+1.09	*	+0.81	*
7	Košetice, CZE	1403	+1.02	*	+14.29	4: I. II. III. VI	+1.21	*	+0.69	
8	Tartu-Tõravere, EST	1210	+0.56		+7.33	3: II. VI. X	−0.76		+0.34	
9	Sodankylä, FIN	818	+1.03	*	+8.30	2: IV. VI	n.a.		+0.04	
10	Lille, FRA	1291	+0.75	*	+9.94	1: V	+1.57	*	+0.87	
11	Observatoire de Haute Provence, FRA	2078	+0.08		+1.56	2: I. XI	+0.89	*	+0.38	
12	Dortmund, GER	1322	+2.00	*	+26.37	9: II. III. IV. V. VI. VIII. IX. X. XI	+1.54	*	+1.35	*
13	Thessaloniki, GRE	2218	+0.46	*	+10.30	1: X	+0.80	*	+0.53	
14	Budapest, HUN	1617	−0.40		−6.52	1: II	+1.05	*	+0.95	*
15	Aosta, ITA	2016	+0.70	*	+14.25	5: II. IV. V. VII. IX	+4.67	*	+0.93	
16	Lampedusa, ITA	2633	−0.02		−0.61	2: XI. XII	+0.56	*	+0.17	
17	Rome, ITA	n.a.	+0.93	*	n.a.	5: II. III. VI. VII. X	+0.98	*	+0.76	
18	Sesto Fiorentino/Florence, ITA	1856	+0.95	*	+17.50	6: I. II. III. VI. VII. X	+1.17	*	+0.81	
19	Bilthoven, NED	1247	+1.80	*	+21.83	4: V. VI. IX. XI	+1.34	*	+1.02	
20	Bergen, NOR	886	+1.03		+9.14	3: IV. VIII. XII	−0.90		+1.16	*
21	Landvik, NOR	1108	+1.08	*	+11.96	2: IV. VIII	−0.48		+0.99	
22	Trondheim, NOR	881	+0.84	*	+7.36	3: IV. VI. XII	−0.32		+0.36	
23	Belsk, POL	1293	+0.66	*	+8.47	1: II	+1.01	*	+0.55	
24	Moscow, RUS	1197	+0.79	*	+9.43	3: VI. VII. X	−0.15		+0.03	
25	Novi Sad, SER	1855	+0.19		+3.61	2: I. II	+1.02	*	+0.93	*
26	Poprad-Ganovce, SVK	1509	+2.15	*	+32.44	8: I. II. VI. VII. VIII. IX. X. XI	+1.11	*	+0.93	*
27	A Coruna, ESP	2115	+1.76	*	+37.34	7: I. II. III. V. IX. XI. XII	+0.87	*	+0.28	
28	Badajoz, ESP	2627	−0.16		−4.13	0:	+0.65	*	+0.72	
29	Barcelona, ESP	2274	−0.04		−0.86	1: VI	+0.54	*	−0.29	
30	Huelva/El Arenosillo, ESP	2830	+0.33		+9.19	2: VI. VII	+0.69	*	+0.68	*
31	Madrid, ESP	2592	−0.29		−7.56	1: II	+0.68	*	−0.15	
32	Malaga, ESP	2696	−0.27		−7.33	0:	+0.59	*	+0.30	
33	Valencia, ESP	2438	−0.04		−1.09	1: II	+0.46	*	+0.22	
34	Davos, CHE	1983	+0.75	*	+14.95	2: V. VI	+2.28	*	+1.19	*
35	Camborne, GBR	1279	+2.61	*	+33.43	10: I. II. III. IV. V. VII. VIII. X. XI. XII	+0.96	*	+0.47	
36	Chilton, GBR	1284	+1.33	*	+17.04	4: I. II. V. VIII	+0.99	*	+0.51	
37	Glasgow, GBR	968	+2.42	*	+23.45	7: I. III. IV. VI. VII. VIII. IX	−0.06		+0.78	

Table 2 (continued)

No.	Location	H					H		H	
		GB					TEMIS		OMI	
		Mean [J_{ery}/ m²]	k [%/yr]	sig.	k [J_{ery} /m²/yr]	Sig. months	k [%/yr]	Sig.	k [%/yr]	Sig.
38	Lerwick, GBR	822	+1.25	*	+10.28	3: I. VI. IX	−1.17		+0.59	
39	Manchester, GBR	967	+0.89	*	+9.03	3: I. IV. VIII	+1.00	*	+0.24	
40	Reading, GBR	1301	+1.45	*	+18.77	7: I. II. III. IV. V. VI. IX	+1.02	*	+0.24	

No.	Location	TOC			GSR		GSR		SSD		SSD	
		OMI			CLARA		SARAH		GB		SARAH	
		k [%/yr]	Sig.	Sig. months	k [%/yr]	Sig.	k [%/yr]	Sig.	k [%/yr]	Sig.	k [%/yr]	Sig.
1	Dornbirn, AUT	−0.04		0:	+1.46	*	+1.34	*	+0.87		+1.50	*
2	Sonnblick, AUT	−0.03		0:	+1.01	*	−0.01		+0.80		−0.66	
3	Wien, AUT	−0.02		0:	+1.07	*	+0.87	*	+0.64	*	+1.49	*
4	Uccle, BEL	−0.04		1: XI	+1.49	*	+1.19	*			+1.80	*
5	Brno-Kotlářská, CZE	−0.02		0:	+1.46	*	+0.94	*	+3.38	*	+1.83	*
6	Hradec Králové, CZE	−0.03		0:	+1.21	*	+0.75	*	+0.96		+1.27	
7	Košetice, CZE	−0.03		0:	+1.40	*	+1.13	*	+2.13	*	+1.72	*
8	Tartu-Tõravere, EST	+0.02		1: V	+0.54		+0.22		−0.47		−0.11	
9	Sodankylä, FIN	−0.01		0:	+0.33		n.a		+1.33		n.a.	
10	Lille, FRA	−0.04		0:	+1.53	*	+1.12	*			+1.58	*
11	Observatoire de Haute Provence, FRA	−0.04		0:	+0.60	*	+0.26				+0.25	
12	Dortmund, GER	−0.03		1: XII	+1.61	*	+1.20	*			+1.82	*
13	Thessaloniki, GRE	−0.01		1: I	+0.67	*	+0.36	*			+0.75	*
14	Budapest, HUN	−0.02		0:	+1.17	*	+0.81	*			+1.70	*
15	Aosta, ITA	−0.04		0:	+1.10	*	+0.56	*	+0.93	*	+0.50	
16	Lampedusa, ITA	−0.02		1: I	−0.04		−0.04		+1.70	*	−0.01	
17	Rome, ITA	−0.03		0:	+0.73	*	+0.33				+0.46	
18	Sesto Fiorentino/Florence, ITA	−0.04		0:	+1.07	*	+0.68	*	+1.55	*	+1.24	*
19	Bilthoven, NED	−0.04		0:	+1.35	*	+0.99	*	+1.97	*	+1.48	*
20	Bergen, NOR	−0.02		1: XII	+1.02	*	+0.10				−0.47	
21	Landvik, NOR	−0.03		2: X. XII	+0.47		+0.52		+1.95	*	+0.51	
22	Trondheim, NOR	−0.01		0:	+0.23		−0.31				−1.21	
23	Belsk, POL	−0.01		0:	+1.08	*	+0.80	*	+2.34	*	+1.12	
24	Moscow, RUS	+ 0.01		2: II. V	+0.52		+0.13		−0.40		−0.09	
25	Novi Sad, SER	−0.02		0:	+0.96	*	+0.71	*	+2.40	*	+1.10	*
26	Poprad-Ganovce, SVK	−0.01		0:	+1.30	*	+1.12	*	+1.99	*	+1.70	*
27	A Coruna, ESP	−0.02		0:	+0.42	*	+0.40	*	+1.20	*	+0.71	*
28	Badajoz, ESP	−0.01		0:	+0.09		+0.05		+0.25		−0.03	
29	Barcelona, ESP	−0.03		0:	−0.35		−0.22		−0.03		−0.31	
30	Huelva/El Arenosillo, ESP	−0.00		0:	+0.20		+0.16		+0.43		+0.15	
31	Madrid, ESP	−0.02		0:	+0.06		−0.18		−0.15		−0.47	
32	Malaga, ESP	−0.01		0:	3−0.36		−0.08		−0.38		−0.35	

Table 2 (continued)

No.	Location	TOC			GSR		GSR		SSD		SSD	
		OMI			CLARA		SARAH		GB		SARAH	
		k [%/yr]	Sig.	Sig. months	k [%/yr]	Sig.	k [%/yr]	Sig.	k [%/yr]	Sig.	k [%/yr]	Sig.
33	Valencia, ESP	−0.01		0:	−0.60		−0.37		+0.35		−0.61	
34	Davos, CHE	−0.03		0:	+1.64	*	+1.11	*	+1.64	*	+1.00	*
35	Camborne, GBR	−0.04		0:	+0.81	*	+0.55	*			+0.76	
36	Chilton, GBR	−0.03		1: XII	+0.93	*	+0.58	*			+0.85	
37	Glasgow, GBR	−0.04		0:	+0.59	*	+0.20				+0.31	
38	Lerwick, GBR	−0.03		0:	+0.05		+0.14				+0.15	
39	Manchester, GBR	−0.04		0:	+0.90	*	+0.37		−0.50		+0.44	
40	Reading, GBR	−0.03		2: XI. XII	+0.94	*	+0.55		+1.75	*	+0.56	

K denotes the trend and significant trends are marked with *

(11/40). For all other months the fraction is within 6 to 10 of 40. This denotes also that in some months the significant increases are spread over a wider geographical region than in others. Table 2 lists the number of months with significant short-term-trends for each location: all significant trends are positive. The number of months with a significant trend varies between 0 and 10 (Fig. 3b) depending on location. Out of the 40 locations, there are only 2 locations (Bajadoz and Malaga, Spain) which have no significant short-term-trend in any month. At more than half of the locations (58%) the monthly mean H_{GB} increases significantly in 1 to 3 months, at almost a quarter (23%) in 4 to 6 months and at 1/7 of locations (14%) H_{GB} increases in more than 6 months.

Figure 4 depicts the annual variability of the significant short-term-trends in monthly mean H_{GB}. The median (black line) ranges between +1.8%/yr and +3.6%/yr. Lowest trends vary between +0.6%/yr and +2.4%/yr and highest trends range from +2.5%/yr to +7.6%/yr. The blue dots indicate all locations having a significant trend in this month. As their number is smaller than 26 (number of stations with significant trend in annual mean), the increase of the annual means is rather caused by significant increases in certain months and not a significant increase over the whole year. Therefore, these monthly trends are higher than that of the annual mean.

Six stations provided even longer series without the need for substituting any of the monthly mean values. For these stations additional trend analysis of annual means was performed for 10-year periods by going back in time year by year, e.g. analyzing 2021-2012, 2020-2011, and so on until statistically significance vanishes. The earliest statistically significant trend (see Table 3) could be detected for the period 2006–2015 in Uccle. However, most stations show a trend onset between 2010 and 2013 (see Table 3).

3.2 Trend analysis of daily UV radiant exposure from OMI

Linear regression analysis of H_{OMI} over the period from 2013 to 2022 delivers a statistically significant trend in the annual mean values for 12 out of 40 locations (Table 2). For these stations, the short-term-trends are all positive, being +0.94%/yr in median (+0.68%/yr to +1.35%/yr) corresponding to +16.6 $J_{ery}/m^2/yr$ (converted as above). On a monthly basis (Fig. 3a, yellow columns), a statistically significant increase is found most frequently in January (26/39), February (26/40) and June (22/40) while for all other months the frequency is < 10/40. Analysis provides fewer significant annual trends for H_{OMI} but more significant monthly trends than for H_{GB} and generally supports the findings from the analysis of H_{GB}.

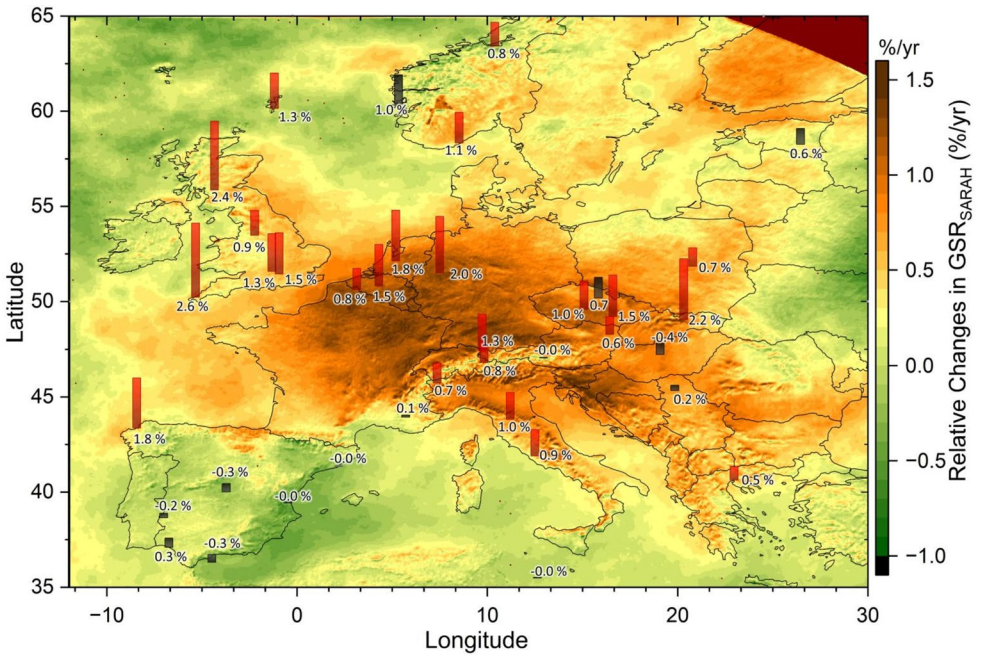


Fig. 2 Relative trends in annual mean H_{GB} per year (red columns: significant; grey columns: insignificant) underlaid by the relative trend in GSR_{SARAH}

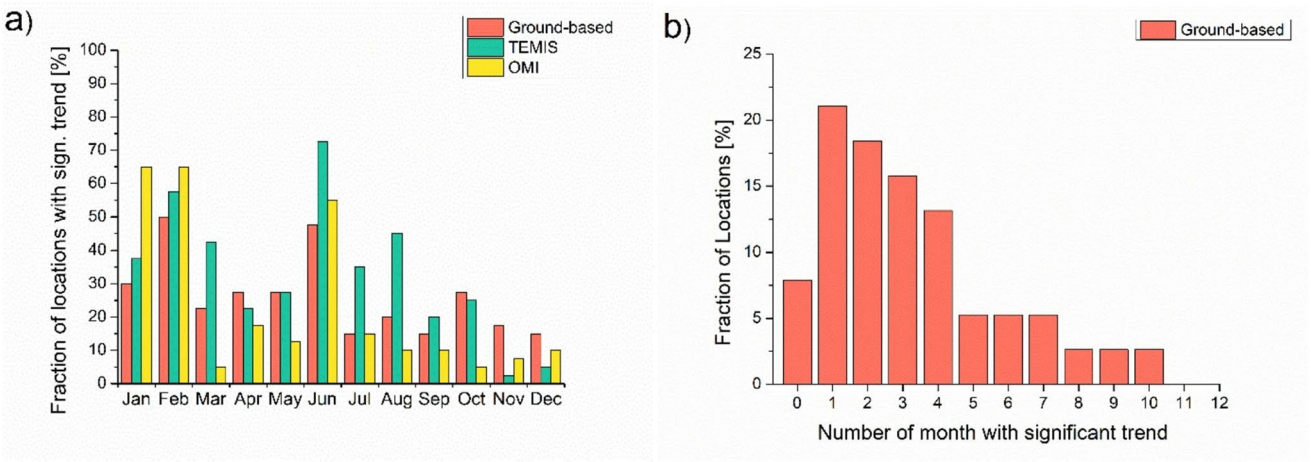


Fig. 3 **a** Fraction of locations with significant trends in monthly mean H_{GB}, H_{TEMIS} and H_{OMI} for each calendar month and **b** fraction of locations with a certain number of months with significant trend in H_{GB} (both over the period from 2013 to 2022)

3.3 Trend analysis of daily UV radiant exposure from TEMIS

Linear regression analysis of H_{TEMIS} for the period from 2013 to 2022 delivers a statistically significant short-term-trend in the annual mean values for 32 out of 39 locations (Table 2), all positive too. Median increase is +1.02%/yr (+0.46%/yr to +4.67%/yr), corresponding to +19.1 J_{ery}/m^2/yr (converted as above). Statistically significant increase (Fig. 3a, green columns) is found most frequently for the period of June (29/39), July (14/39) and August (18/39) as well as for the period of January (15/38), February (23/39), and March (17/39). Also, this data set shows general agreement with findings from H_{GB}.

3.4 Trend analysis of total ozone column

To investigate if ongoing changes in total ozone column (TOC) may have influenced H_{GB}, linear regression analysis was performed on monthly and annual mean TOC (2013–2022) over all stations. In total, there was no statistically significant short-term trend in the annual mean TOC (see Table 2) for any location. The derived TOC trends range between −0.04%/yr to +0.02%/yr, with negative values in 38 cases out of 40. For 10 locations, significant trends - all positive - were found for some calendar months (Jan: 2/38, Feb.: 1/40, May: 2/40, Oct.:1/40, Nov.: 2/40, Dec.: 5/37) which could cause a decrease in H_{GB}, and weaken the overall increasing trend in H_{GB}.

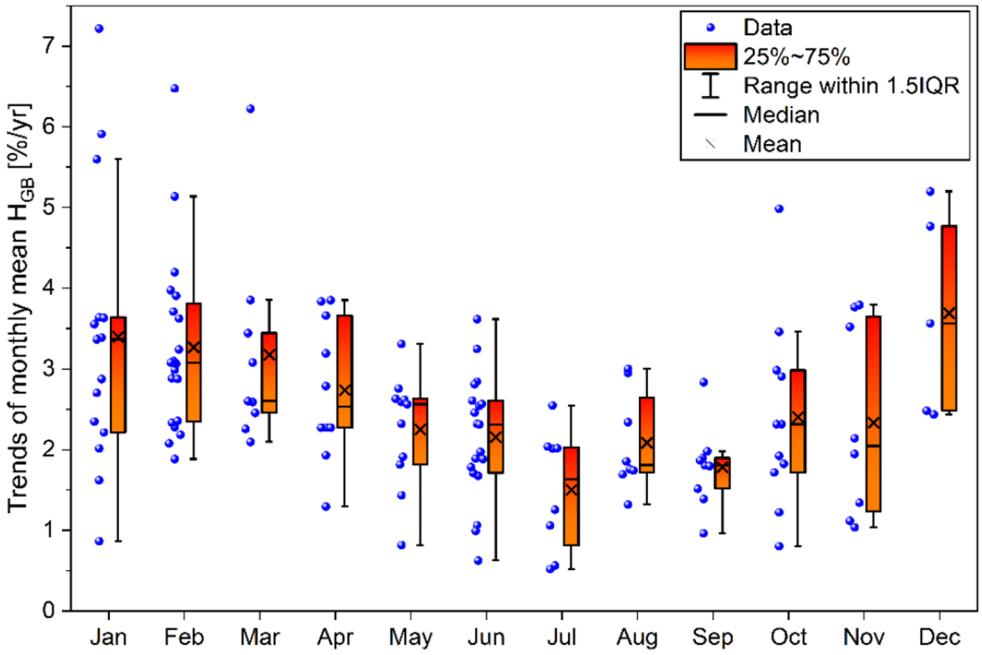


Fig. 4 Trends of monthly means for each calendar month (statistically significant trends only) (blue dots). The boxes indicate the 25%−75% range of trends, the black line the Median, the "x" the mean and the error bars the 1.5 interquartile range (1.5 IQR)

Table 3 Earliest periods with significant 10-year-trends for observatories with gap-free long-term series

Observatory	Time series	Earliest period of sign. trend
Belsk	1976–2024	2013–2022
Dortmund	1997–2023	2010–2019
Landvik	1995–2024	2011–2020
Moscow	2001–2023	2013–2022
Trondheim	1995–2024	2011–2020
Uccle	1991–2023	2006–2015

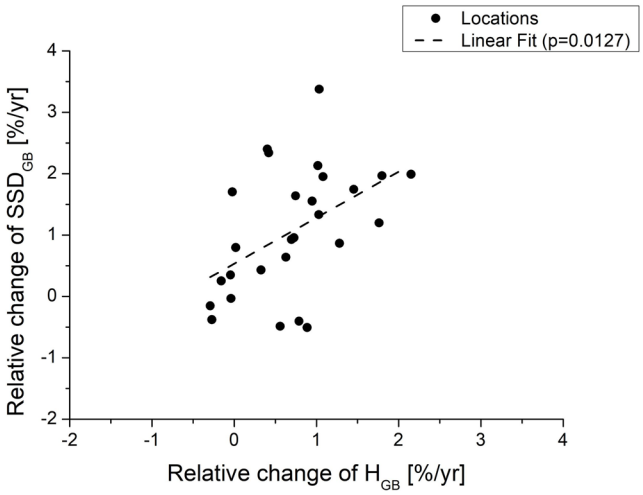


Fig. 5 Changes in annual mean of ground-based sunshine duration SSD_{GB} versus changes in annual mean of H_{GB}

3.5 Trend analysis of sunshine duration measured from ground and from SARAH-3

For 21 of 27 stations, which provided sunshine duration SSD_{GB} (see Table 2), there was an agreement in statistical significance of trends of annual means for SSD_{GB} and H_{GB} (either statistically significant for both or not significant for both). For 4 stations, the trend in H_{GB} was significant but not in SSD_{GB}, and for 2 stations the opposite. Figure 5 depicts the relative change (%/yr) in SDD_{GB} in comparison to the change in H_{GB}. Linear regression analysis provides a statistically significant relation ($p = 0.006$) between both, depicted by the dashed line in Fig. 5. The slope of this line is +0.76 (standard error ± 0.28, $R^2 = 0.19$), denoting that changes in SSD_{GB} and H_{GB} are related close to 1:1, and that changes in H_{GB} can be explained largely by changes in cloud cover. Changes in annual mean SSD_{SARAH} also correlate significantly ($p = 0.038$) with changes in H_{GB}.

Figure 6 illustrates changes in annual mean SSD_{GB} (violet columns) and satellite-based from SARAH (SSD_{SARAH}, blue columns) along with trends in satellite-based GSR from SARAH (GSR_{SARAH}) for all locations (red column) and over Europe (colored map, green to red). Values for all locations are listed in Table 2. Changes in GSR_{SARAH} are lower than for SSD_{SARAH} and are highest for SSD_{GB} at most locations. In the alpine region, SSD_{GB} and SSD_{SARAH} are as variable as GSR_{SARAH} is.

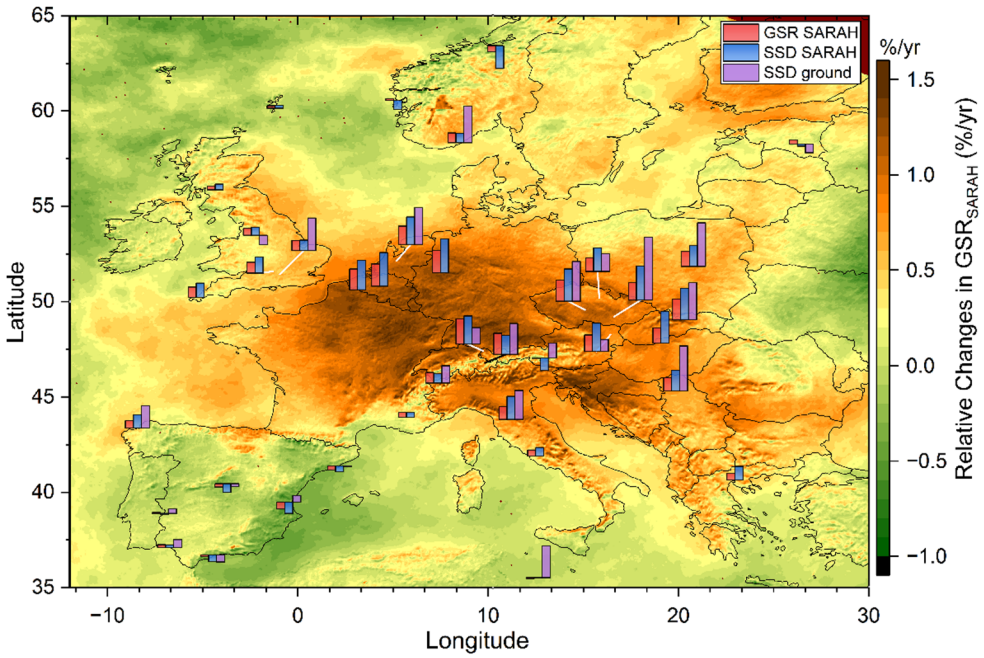


Fig. 6 Relative changes in sunshine duration measured at the ground (SSD ground, violet columns, if available), from space (SSD_{SARAH}, blue columns) and changes in global solar radiation (GSR_{SARAH}, red columns) for all locations underlaid by the relative change in global solar radiation from SARAH

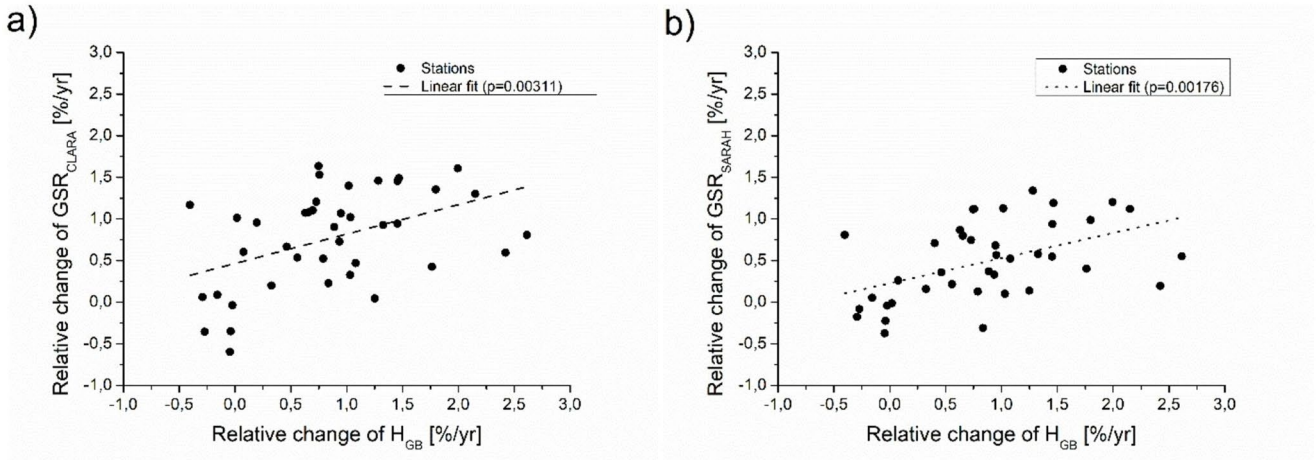


Fig. 7 Relative changes of annual means in ground-based UVR measurements (H_{GB}) compared to relative changes of annual means in global solar radiation gained (**a**) from CLARA (GSR_{CLARA}) and (**b**) from SARAH (GSR_{SARAH})

3.6 Correlation with trends in global solar radiation from CLARA and SARAH

For annual means of GSR_{CLARA} and GSR_{SARAH} linear trend analysis was performed for each location for the period 2013–2022 too. Changes in annual mean GSR_{CLARA} and GSR_{SARAH} are depicted in Fig. 7 with respect to changes in H_{GB}, all changes expressed in % per year. Statistical analysis suggests a significant relation between changes in H_{GB} and GSR_{CLARA} ($p=0.0256$) and GSR_{SARAH} ($p=0.0214$) indicated by the dashed line in both panels. It can be recognized that changes in GSR are only around one third to one half of those in H_{GB}. However, a small number of data points deviate noticeably from the linear relationship (dashed line). Locations with a strong trend in H_{GB} may have little or no change in GSR_{CLARA} and GSR_{SARAH} and vice versa.

4 Discussion

During recent decades, there has been evidence that solar UVR reaching the earth's surface has risen at some locations [16–21]. However, attributing these changes to specific regions or time periods has been challenging. We analysed measurements from 40 stations, all made over the same period, and found that increasing surface UVR is a Europe-wide phenomenon except for the mid- and southern part of the Iberian Peninsula), evident from countries

in the south, such as Greece, up to the mid-part of Scandinavia and from the western British Islands eastwards to countries in eastern Central Europe, such as Poland and Slovakia. Evidence is provided by both ground-based UVR measurements and by satellite UVR products from OMI and TEMIS. At no location were statistically significant annual or monthly decreases found (ground-based and satellite). Further, trends from ground-based UVR measurements correlate with trends of satellite derived GSR. Decreases in total ozone column can be excluded as a cause, as only increases were found in TOC, some of which were statistically significant for a few calendar months at a few locations. In contrast, analysis of SSD points clearly to a reduction of cloud coverage as a cause for the entire area of the study.

This is consistent with the findings of a multi-cause analysis [72] on the role of clouds and aerosols in the global radiation trends in Europe over recent decades, based on various datasets (including SARAH-3, CLARA-A3, among others): The direct effect of aerosols is estimated to contribute approximately 20% to these trends, while cloud-related changes are estimated to account for around 80%. A decrease in near-surface relative humidity, which is expected to decrease in a warming climate [73], can further explain the decrease trends in cloud cover over the continents, as analysed by Liu et al. [74].

One possible factor that may contribute to the high spatial variability of the trends in the Alpine region is the combination of high topographic variability and the influence of snow cover and albedo. The Alpine region is characterized by a complex topography, with steep slopes and varying elevations, which can lead to a high degree of spatial variability in UVR [75]. Additionally, the presence of snow cover in this region, even during the summer months (Fig. 1), may further increase the UVR due to the high albedo of snow. A local decrease of snow cover may partially weaken a UVR trend. Also, the general decreasing cloud trend in central Europe may be influenced by complex topography and altitude in this region. However, the high agreement between the patterns of ground-based UVR measurements and the spatial high-resolution map of satellite-derived GSR trends in this region suggests that this alpine pattern is significant and constitutes one of the key-findings of this study.

The high agreement between the patterns of ground-based UVR measurements and the high-resolution spatial trend map of satellite-derived GSR provides valuable insight into the possibility of transferring local ground-based UVR trends to the surrounding area, and recognizing how far this transfer is plausible. While qualitative agreements exist, our quantitative analyses confirm that high-quality ground-based measurement stations remain irreplaceable by satellite data for precise assessments of ground-level UVR changes. However, the combination of both provides a plausible and complete picture of UVR trends across countries and the entire continent, offering a comprehensive understanding of the spatial and temporal patterns of UVR changes. Significant changes in annual means were estimated to range from +4.6% to +26% over the decade from 2013 to 2022 (median is +11.2%/dec). On average, mean daily H_{GB} is around 14 SED (1400 J/m²) and increased over the 10-year period by 0.17 SED per year respectively 1.7 SED over the considered decade. Although numeric values are estimated from a 10-year period, the high number of locations provides a valid and robust estimate. And even though we deliberately selected a period with a strong expected increase and a strong gradient in Europe to identify patterns and boundaries very well, this increase is relevant for quantitative discussion. The increase rates are of the order of magnitude as previously reported for a few locations in Europe [16–21].

Analysis of longer time series from six observatories in this study showed that trends have become significant between 2010 and 2013 but not all at the same time and with the exception of Uccle, which exhibits notably low year-to-year fluctuations [21]. To determine the start date of the increase, more efforts are necessary to reprocess measurements, which often started in the late 1990 s [25], and apply gap filling methods - like those by Johnsen et al. [38] or Heinzl et al. [48] - to achieve high quality data that go back to the start date of UVR monitoring.

The trends in annual means do not indicate a uniform trend across the year but are driven by changes in particular calendar months that are then noticeably higher than those of annual means. The greatest change of monthly means (Fig. 4) from 2013 to 2022 were found for November, December and January with a magnitude of around 4%/yr in northern European countries, perhaps indicative of a snow-cover-influence. The smallest percentage increases were found in summer months with around 2%/yr. A trend was found for at least one station for all calendar months, but trends were most frequently observed in January and February as well as in June. The summer months are particularly relevant for radiation protection, as they have the highest UVR in Europe and therefore the greatest impact on health. The contribution of the monthly UVR to the annual mean differs significantly among months. For example, at Vienna (48°N), December and January contribute only 1% each to the annual total, due to low solar elevation, fewer day light hours and high cloudiness, while July contributes 19%. At more northern locations the contribution of winter months to the annual total may be even less.

The implications of the observed increases in UVR exposure on humans are hard to estimate, because there is a lack in dose-response relationships for most UVR-related effects. Best known is the relation between UVR and Non-Melanoma skin cancer (NMSC). Available models estimate

the incidence of NMSC by including genetic disposition, exposed body surface area, age and annual radiant exposure [76, 77]. The annual radiant exposure contributes by the power of 1.7 to 3.0 [78–81] depending on type of NMSC and gender. Assuming a power of 2, the estimated range of increase in annual radiant exposure of 6% to 26% (median 11%) simply squares and could lead to an increase (with corresponding latency period) in the incidence rate of NMSC of between 9% and 59% (median 24%), assuming populations (e.g. age distribution) and their behaviour do not change (travel patterns, time spent outdoors, sun exposure habits,.). Consequently, projections of skin cancer incidence remain subject to considerable uncertainty. Nevertheless, the additional UVR burden necessitates behavioural adaptations–such as modified outdoor activities or increased usage of protective measures-and requires active public health communication.

Beyond human health, the observed UVR increase influences terrestrial and aquatic ecosystems, affecting photosynthetic balance and agricultural productivity. The complex interplay between such ecological impacts necessitates to interpret UVR trends within a comprehensive multifaceted framework rather than separated.

The findings of our study have direct implications for the achievement of several United Nations Sustainable Development Goals (SDGs). Firstly, our research contributes to SDG 3 (Good Health and Well-being) by providing critical data that can inform public health strategies aimed at minimizing health risks associated with increased UVR exposure. By identifying regions with significant UVR increases, targeted interventions, public health advisories, and educational campaigns can be developed to mitigate health impacts. Secondly, the enhanced understanding of UVR patterns supports SDG 11 (Sustainable Cities and Communities) by guiding urban planning and policymaking to ensure cities develop in ways that protect residents from UV-related health risks, thereby promoting safer and healthier communities. Furthermore, our study informs SDG 13 (Climate Action) by providing insights into how changes in climate patterns, such as cloud cover reduction, influence surface UVR levels. This knowledge is crucial for developing strategies to adapt to and mitigate the effects of climate change including agriculture (SDG 2). Lastly, by highlighting the broader ecological consequences of increased UVR, such as potential impacts on biodiversity, our research supports SDG 15 (Life on Land). Protecting ecosystems and understanding anthropogenic and natural changes to these systems are crucial for sustainable management and conservation efforts.

5 Conclusion

In conclusion, our study provides strong evidence for a Europe-wide increase in surface UVR under all-sky conditions over the past decade(s), with significant trends of annual mean UVR observed at 26 out of 40 locations between 2013 and 2022. These statistically significant trends range between +0.46% and +2.62% per year and are higher in central Europe and lower in the south and north of Europe. The good agreement between ground-based UVR measurements and satellite-derived GSR trends suggests that local trends can be extrapolated to the surrounding area, providing a comprehensive understanding of the spatial and temporal patterns of UVR changes. Our results indicate that the increase in UVR is primarily driven by a reduction in cloudiness. As can be inferred from the analysis of sunshine duration data, the effects of aerosols are generally small and masked by the effects of clouds and there are only very minor effects from the observed changes in TOC.

The implications of this increase on living organisms, including human health, are significant, with an expected rise in non-melanoma skin cancer incidence. Given the potential photomedical and photobiological implications of these changes, it is essential to continue monitoring UVR and to expand our understanding of the underlying mechanisms driving these changes. To achieve this, the following steps are necessary:

- Longer time series from more measuring sites need to be processed to determine the start date of the increase, to better understand the underlying mechanisms driving these changes, and to enhance spatial information.
- Continued monitoring with well-defined QA/QC procedures is necessary to monitor further developments of UVR and to provide early warnings of potential health risks.
- Processed time series data should be made available for impact research, to facilitate the development of effective strategies to mitigate the adverse effects of UVR on human health and the environment.

By taking these steps, we can improve our understanding of UVR trends and their implications for human health and the environment and develop effective strategies to mitigate the adverse effects of UVR. Our research contributes to the achievement of several United Nations Sustainable Development Goals (SDGs), including Good Health and Well-being, Sustainable Cities and Communities, Climate Action, and Life on Land, by providing critical insights into the trends and implications of UVR for human health and the environment.

Acknowledgements The authors would like to acknowledge the following individuals, institutions, and agencies for their contributions to this study: We thank the Austrian Federal Ministry for Agriculture and Forestry, Climate and Environmental Protection, Regions and Water Management for funding the measurements at Dornbirn, Vienna and Sonnblick. The research at the Brno-Kotlářská station was funded by the Ministry of Education, Youth and Sports (Project VAN 2025). We acknowledge the Ministry of the Environment of the Czech Republic and Czech hydrometeorological institute (CHMU) for funding and organizing the UV network in the Czech Republic. We thank the Estonian Environment Agency for providing the Tartu-Tõravere station data used in this study. The work at Sodankylä was partly supported by the Research Council of Finland grant no. 368143 (GUVIR-project). We thank Tomi Karppinen and Juha M. Karhu for the operation of the Brewer in Sodankylä. We acknowledge the support of the Région Hauts-de-France and the Ministère de l'Enseignement Supérieur et de la Recherche (via CPER Climibio) and the ACTRIS (Aerosol, Clouds, and Trace Gases Research Infrastructure) for providing access to high-quality data, facilities, and technical support that were integral to the execution of the research at Lille-Villeneuve d'Ascq and Obs. de Haute Provence. We thank Marco Janßen, Günther Ott, and Stefan Bauer from the Federal Institute for Occupational Safety and Health for operating the Bentham in Dortmund. The measurements at Lampedusa have been supported by the Italian Ministry for University and Research through projects NextData, Marine Hazard, and PER-ACTRIS-IT, and by the EC-Valmed.it project, funded by the Italian Space Agency. Contributions by Damiano Sferlazzo at Lampedusa are gratefully acknowledged. The measurements in Rome were funded by "Progetti di Ricerca Grandi" of Sapienza University of Rome (Prot. RG123188AFDE2E0D). We thank Anak Bhandari, Geophysical Institute, University of Bergen, for operating the station at Bergen. Thanks to operator Lars T. Havstad, Norwegian Institute of Bioeconomy Research, for operating the station at Landvik. We also thank Osvaldo Trigueiro Neto, Norwegian University of Science and Technology (NTNU), for operating the station at Trondheim. The research at Belsk was financially supported by the Chief Inspectorate of Environmental Protection (grant no. GIOŚ/247/2025/DMŚ/NFOŚ). We acknowledge the Slovak hydrometeorological institute (SHMU) for organizing the UV network at Poprad-Ganovce. We thank J. M. San Atanasio, responsible for the AEMET's radiometric laboratory, and P. Fernandez, responsible for the network, for their contributions at A Coruna, Badajoz, Barcelona, Huelva, Madrid, Malaga, and Valencia. The project at INTA/El Arenosillo (Huelva) was also funded by the PID2023-149390OB-C22 R+D+I project, funded by MI CIU/AEI/10.13039/501100011033/and "ERDF A Way of Doing Europe". We acknowledge the support of Geosphere Austria for providing global solar radiation data for Dornbirn and Sonnblick, and MeteoSwiss for providing sunshine duration data for Davos, Switzerland. Spectral ultraviolet radiation and ozone measurements at Manchester and Reading were managed by University of Manchester and funded by UK Department of Environment Food and Rural Affairs (DEFRA). We thank University of Reading for hosting equipment at their Atmospheric Observatory. Sunshine duration data were supplied by the Whitworth Meteorological Observatory at University of Manchester and by Reading University Atmospheric Observatory for Manchester and Reading sites, respectively.

Author contributions A.S. wrote the main manuscript text and prepared figuresS.L. wrote the main manuscript text and prepared figuresD.K. statistical analysis and prepared figuresAll others: prepared quality controlled time series and contributed with data related informationAll authors reviewed the manuscript.

Funding Open access funding provided by University of Veterinary Medicine Vienna

Data availability Data are available upon request.

Declarations

Conflict of interest The authors declare no competing interests.

Open Access This article is licensed under a Creative Commons Attribution 4.0 International License, which permits use, sharing, adaptation, distribution and reproduction in any medium or format, as long as you give appropriate credit to the original author(s) and the source, provide a link to the Creative Commons licence, and indicate if changes were made. The images or other third party material in this article are included in the article's Creative Commons licence, unless indicated otherwise in a credit line to the material. If material is not included in the article's Creative Commons licence and your intended use is not permitted by statutory regulation or exceeds the permitted use, you will need to obtain permission directly from the copyright holder. To view a copy of this licence, visit http://creativecommons.org/licenses/by/4.0/.

References

1. di Sarra, A., Cacciani, M., Chamard, P., Cornwall, C., DeLuisi, J. J., Di Iorio, T., Disterhoft, P., Fiocco, G., Fua, D., & Monteleone, F. (2002). Effects of desert dust and ozone on the ultraviolet irradiance at the Mediterranean island of Lampedusa during PAUR II. *Journal of Geophysical Research, 107*, Article 8135. https://doi.org/10.1029/2000JD000139
2. Chatzopoulou, A., Tourpali, K., Bais, A. F., & Braesicke, P. (2025). Effects of different aerosol types on surface UV radiation in the 21st century. *Atmospheric Environment, 362*, Article 121595. https://doi.org/10.1016/j.atmosenv.2025.121595
3. Németh, P., Tóth, Z., & Nagy, Z. (1996). Effect of weather conditions on UV-B radiation reaching the earth's surface. *Journal of Photochemistry and Photobiology. B, Biology, 32*(3), 177–181. https://doi.org/10.1016/1011-1344(95)07221-7
4. Kylling, A., Dahlback, A., & Mayer, B. (2000). The effect of clouds and surface albedo on UV irradiances at a high latitude site. *Geophysical Research Letters, 27*(9), 1411–1414. https://doi.org/10.1029/1999GL011015
5. Simic, S., Fitzka, M., Schmalwieser, A., Weihs, P., & Hadzimustafic, J. (2011). Factors affecting UV irradiance at selected wavelengths at Hoher Sonnblick. *Atmospheric Research, 101*(4), 869–878. https://doi.org/10.1016/j.atmosres.2011.05.022
6. Schmalwieser, A. W., Weihs, P., & Schauberger, G. (2018). UV Effects on Living Organisms. In R. Meyers (Ed.), *Encyclopedia of Sustainability Science and Technology* (pp. 1–63). Springer. https://doi.org/10.1007/978-1-4939-2493-6_454-3
7. De Winter, S., Vink, A. A., Roza, L., & Pavel, S. (2001). Solar-simulated skin adaptation and its effect on subsequent UV-induced epidermal DNA damage. *The Journal of Investigative Dermatology, 117*, 678–682.
8. Martinez-Levasseur, L., Birch-Machin, M., Bowman, A., Gendron, D., Weatherhead, E., Knell, R. J., & Acevedo-Whitehouse, K. (2013). Whales use distinct strategies to counteract solar ultraviolet radiation. *Scientific Reports, 3*, Article 2386. https://doi.org/10.1038/srep02386
9. D'Ambrosio, S. M., Whetstone, J. W., Slazinski, L., & Lowney, E. (1981). Photorepair of pyrimidine dimers in human skin in vivo. *Photochemistry and Photobiology, 34*(4), 461–464.
10. Tang, X., Yang, T., Yu, D., Xiong, H., & Zhang, S. (2024). Current insights and future perspectives of ultraviolet radiation (UV) exposure: Friends and foes to the skin and beyond the skin.

Environment International, 185, Article 108535. https://doi.org/10.1016/j.envint.2024.108535
11. Arnold, M., Singh, D., Laversanne, M., Vignat, J., Vaccarella, S., Meheus, F., Cust, A. E., de Vries, E., Whiteman, D. C., & Bray, F. (2022). Global burden of cutaneous melanoma in 2020 and projections to 2040. *JAMA Dermatology, 158*(5), 495–503. https://doi.org/10.1001/jamadermatol.2022.0160
12. Bray, F., Laversanne, M., Sung, H., Ferlay, J., Siegel, R. L., Soerjomataram, I., & Jemal, A. (2024). Global cancer statistics 2022: GLOBOCAN estimates of incidence and mortality worldwide for 36 cancers in 185 countries. *CA: A Cancer Journal for Clinicians, 74*(3), 229–263. https://doi.org/10.3322/caac.21834
13. Green, A. C., & Olsen, C. M. (2017). Cutaneous squamous cell carcinoma: An epidemiological review. *British Journal of Dermatology, 177*(2), 373–381. https://doi.org/10.1111/bjd.15324
14. Verkouteren, J. A. C., Ramdas, K. H. R., Wakkee, M., & Nijsten, T. (2017). Epidemiology of basal cell carcinoma: Scholarly review. *British Journal of Dermatology, 177*(2), 359–372. https://doi.org/10.1111/bjd.15321
15. Brokmeier, L. L., Ilic, L., Haas, S., Uter, W., Heppt, M. V., Gefeller, O., & Kaiser, I. (2025). Knowledge and risk perception regarding keratinocyte carcinoma in lay people: A systematic review and meta-analysis. *Healthcare, 13*(15), Article 1912. https://doi.org/10.3390/healthcare13151912
16. De Bock, V., De Backer, H., Van Malderen, R., Mangold, A., & Delcloo, A. (2014). Relations between erythemal UV dose, global solar radiation, total ozone column and aerosol optical depth at Uccle, Belgium. *Atmospheric Chemistry and Physics*, *14*(22), 12251–12270. https://doi.org/10.5194/acp-14-12251-2014
17. Fountoulakis, I., Zerefos, C. S., Bais, A. F., Kapsomenakis, J., Koukouli, M.-E., Ohkawara, N., Fioletov, V., De Backer, H., Lakkala, K., Karppinen, T., & Webb, A. R. (2018). Twenty-five years of spectral UV-B measurements over Canada, Europe and Japan: Trends and effects from changes in ozone, aerosols, clouds, and surface reflectivity. *Comptes Rendus Geoscience, 350*(7), 393–402. https://doi.org/10.1016/j.crte.2018.07.011
18. Čížková, K., Láska, K., Metelka, L., & Staněk, M. (2018). Reconstruction and analysis of erythemal UV radiation time series from Hradec Králové (Czech Republic) over the past 50 years. *Atmospheric Chemistry and Physics, 18*, 1805–1818. https://doi.org/10.5194/acp-18-1805-2018
19. Fountoulakis, I., Diémoz, H., Siani, A.-M., Laschewski, G., Filippa, G., Arola, A., Bais, A. F., De Backer, H., Lakkala, K., Webb, A. R., De Bock, V., Karppinen, T., Garane, K., Kapsomenakis, J., Koukouli, M.-E., & Zerefos, C. S. (2020). Solar UV irradiance in a changing climate: Trends in Europe and the significance of spectral monitoring in Italy. *Environments, 7*(1), Article 1. https://doi.org/10.3390/environments7010001
20. Fountoulakis, I., Diémoz, H., Siani, A. M., di Sarra, A., Meloni, D., & Sferlazzo, D. M. (2021). Variability and trends in surface solar spectral ultraviolet irradiance in Italy: On the influence of geopotential height and lower-stratospheric ozone. *Atmospheric Chemistry and Physics, 21*(24), 18689–18705. https://doi.org/10.5194/acp-21-18689-2021
21. Lorenz, S., Heinzl, F., Bauer, S., Janßen, M., De Bock, V., Mangold, A., Scholz-Kreisel, P., & Weiskopf, D. (2024). Increasing solar UV radiation in Dortmund, Germany: Data and trend analyses and comparison to Uccle, Belgium. *Photochemical & Photobiological Sciences, 23*(12), 2173–2199. https://doi.org/10.1007/s43630-024-00658-8
22. Czerwińska, A., Krzyścin, J., Jarosławski, J., Sobolewski, P. S., & Pietruczuk, A. (2025). Trends in the erythemal radiant exposure from re-evaluated measurements (1976–2023) with biometers in Belsk, Poland, and their sources from corresponding ozone, aerosol, and cloud observations. *Atmospheric Chemistry and Physics, 25*, 12497–12512. https://doi.org/10.5194/acp-25-12497-2025
23. Lakkala, K., Heikkilä, A., Kärhä, P., Ialongo, I., Karppinen, T., Karhu, J. M., Lindfors, A. V., & Meinander, O. (2017). 25 years of spectral UV measurements at Sodankylä. In: Radiation processes in the atmosphere and ocean (IRS2016) AIP Conference Proceedings, 1810. https://doi.org/10.1063/1.4975568
24. Hunter, N., Rendell, R. J., Higlett, M. P., O'Hagan, J. B., & Haylock, R. G. E. (2019). Relationship between erythema effective UV radiant exposure, total ozone, cloud cover and aerosols in southern England, UK. *Atmospheric Chemistry and Physics*, *19*(1), 683–699. https://doi.org/10.5194/acp-19-683-2019
25. Schmalwieser, A. W., Gröbner, J., Blumthaler, M., Klotz, B., De Backer, H., Bolsée, D., Werner, R., Tomsic, D., Metelka, L., Eriksen, P., Jepsen, N., Aun, M., Heikkilä, A., Duprat, T., Sandmann, H., Weiss, T., Bais, A., Toth, Z., Siani, A. M., Vaccaro, L., Diémoz, H., Grifoni, D., Zipoli, G., Lorenzetto, G., Petkov, B. H., di Sarra, A. G., Massen, F., Yousif, C., Aculinin, A. A., den Outer, P., Svendby, T., Dahlback, A., Johnsen, B., Biszczuk-Jakubowska, J., Krzyscin, J., Henriques, D., Chubarova, N., Kolarž, P., Mijatovic, Z., Groselj, D., Pribullova, A., Gonzales, J. R. M., Bilbao, J., Guerrero, J. M. V., Serrano, A., Andersson, S., Vuilleumier, L., Webb, A., & O'Hagan, J. (2017). UV Index monitoring in Europe. *Photochemical & Photobiological Sciences*, *16*(9), 1349–1370. https://doi.org/10.1039/c7pp00178a
26. Webb, A., Gröbner, J., & Blumthaler, M. (2006). *A Practical Guide to Operating Broadband Instruments Measuring Erythemally Weighted Irradiance*. Office for Official Publications of the European Communities.
27. Goessling, H. F., Rackow, T., & Jung, T. (2025). Recent global temperature surge intensified by record-low planetary albedo. *Science, 387*(6729), 68–73. https://doi.org/10.1126/science.adq7280
28. Urraca, R., Trentmann, J., Pfeifroth, U., & Gobron, N. (2024). Can satellite products monitor solar brightening in Europe? *Remote Sensing of Environment, 315*, Article 114472. https://doi.org/10.1016/j.rse.2024.114472
29. Blumthaler, M. (2004). Quality assurance and quality control methodologies used within the Austrian UV monitoring network. *Radiation Protection Dosimetry, 111*(4), 359–362.
30. Schmalwieser, A. W., Eschenbacher, S., & Schreder, J. (2022). UV-Biometer - The usage of erythemal weighted broadband meters for other biological effects. *Journal of Photochemistry and Photobiology B, 230*, 112442. https://doi.org/10.1016/j.jphotobiol.2022.112442
31. Metelka, L. (2018). Clear-sky UV index values for the Czech Republic. *Meteorologické zprávy*, *71*(2), 33–38.
32. Lakkala, K., Arola, A., Heikkilä, A., Kaurola, J., Koskela, T., Kyrö, E., Lindfors, A., Meinander, O., Tanskanen, A., Gröbner, J., & Hülsen, G. (2008). Quality assurance of the Brewer spectral UV measurements in Finland. *Atmospheric Chemistry and Physics, 8*, 3369–3383. https://doi.org/10.5194/acp-8-3369-2008
33. Brogniez, C., Doré, J.-F., Auriol, F., Cesarini, P., Minvielle, F., Deroo, C., Catalfamo, M., Metzger, J.-M., & Da Conceicao, P. (2021). Erythemal and vitamin D weighted solar UV dose-rates and doses estimated from measurements in mainland France and on Réunion Island. *Journal of Photochemistry and Photobiology B, Biology, 225*, Article 112330. https://doi.org/10.1016/j.jphotobiol.2021.112330
34. Lakkala, K., Kujanpää, J., Brogniez, C., Henriot, N., Arola, A., Aun, M., Auriol, F., Bais, A. F., Bernhard, G., De Bock, V., Catalfamo, M., Deroo, C., Diémoz, H., Egli, L., Forestier, J. B., Fountoulakis, I., Garcia, R. D., Gröbner, J., Hassinen, S., … Tamminen, J. (2020). Validation of TROPOMI surface UV radiation product. *Atmospheric Measurement Techniques, 13*, 6999–7024. https://doi.org/10.5194/amt-13-6999-2020
35. Bais, A. F., Topaloglou, C., Kazadzis, A., Blumthaler, M., Schreder, J., Schmalwieser, A. W., Henriques, D., & Janouch, M.

(2001). Report of the LAP/COST/WMO Intercomparison of Erythemal radiometers, Thessaloniki, Greece, 1999. WMO/GAW Report No. 141, WMO/TD No. 1051.
36. di Sarra, A., Fuà, D., Cacciani, M., Di Iorio, T., Disterhoft, P., Meloni, D., Monteleone, F., Piacentino, S., & Sferlazzo, D. (2008). Determination of ultraviolet cosine corrected irradiances and aerosol optical thickness by combined measurements with a Brewer spectrophotometer and a MultiFilter Rotating Shadowband Radiometer. *Applied Optics, 47*, 6142–6150.
37. den Outer, P. N., Slaper, H., Kaurola, J., Lindfors, A., Kazantzidis, A., Bais, A. F., Feister, U., Junk, J., Janouch, M., & Josefsson, W. (2010). Reconstructing of erythemal ultraviolet radiation levels in Europe for the past 4 decades. *Journal of Geophysical Research, 115*, Article D1010. https://doi.org/10.1029/2009JD012827
38. Johnsen, B., Hansen, E. L., Nilsen, L. T., Saxebøl, G., Hoftuft, J., Svendby, T. M., Dahlback, A., Kjeldstad, B., Berge, E., & Hannevik, M. (2025). Three decades of UV-monitoring in Norway: Trends and drivers. DSA Report 2025:03. Norwegian radiation and nuclear safety authority, Østerås, Norway, ISSN 2535-7339.
39. Krzyścin, J. W., Czerwińska, A., Rajewska-Więch, B., Jarosławski, J., Sobolewski, P. S., & Pawlak, I. (2025). Biologically effective daily radiant exposure for erythema appearance, previtamin D_3 synthesis, and clearing of psoriatic lesions derived from erythemal broadband meters at Belsk, Poland, for the period 1976–2023. *Earth System Science Data Discussions, 17*, 3757–3775. https://doi.org/10.5194/essd-17-3757-2025
40. Zhdanova, E. Y., Chubarova, N. Y., & Blumthaler, M. (2014). Biologically active UV-radiation and UV-resources in Moscow (1999–2013). *Geography Environment Sustainability*, *2014*(2), 71–85. https://doi.org/10.24057/2071-9388-2014-7-2-71-85
41. Malinović-Milićević, S., Radovanović, M. M., Mijatović, Z., & Petrović, M. D. (2022). Reconstruction and variability of high daily erythemal ultraviolet doses and relationship with total ozone, cloud cover, and albedo in Novi Sad (Serbia). *International Journal of Climatology*, *42*(16), 9088–9100. https://doi.org/10.1002/joc.780
42. Redondas, A., Carreño, V., León-Luis, S. F., Hernández-Cruz, B., López-Solano, J., Rodriguez-Franco, J. J., Vilaplana, J. M., Gröbner, J., Rimmer, J., Bais, A. F., Savastiouk, V., Moreta, J. R., Boulkelia, L., Jepsen, N., Wilson, K. M., Shirotov, V., & Karppinen, T. (2018). EUBREWNET RBCC-E Huelva 2015 ozone brewer intercomparison. *Atmospheric Chemistry And Physics, 18*, 9441–9455. https://doi.org/10.5194/acp-18-9441-2018
43. Rendell, R., Khazova, M., Higlett, M., & O'Hagan, J. (2021). Impact of high solar UV radiant exposures in spring 2020 on SARS-CoV-2 viral inactivation in the UK. *Photochemistry And Photobiology, 97*, 542–548. https://doi.org/10.1111/php.13401
44. Hooke, R. J., Higlett, M. P., Hunter, N., & O'Hagan, J. (2017). Long term variations in erythema effective solar UV at Chilton, UK, from 1991 to 2015. *Photochemical & Photobiological Sciences*, *16*, 1596–1603. https://doi.org/10.1039/c7pp00053g
45. Smedley, A. R. D., Rimmer, J. S., Moore, D., Toumi, R., & Webb, A. R. (2012). Total ozone and surface UV trends in the United Kingdom: 1979–2008. *International Journal of Climatology, 32*, 338–346. https://doi.org/10.1002/joc.2275
46. EN ISO/CIE 17166. (2019). *Erythema reference action spectrum and standard erythema dose*. European Standards.
47. NASA Earth Observatory (2005). Blue marble: Next generation [Map]. Retrieved from https://science.nasa.gov/earth/earth-observatory/blue-marble-next-generation/ (last access May 2025).
48. Heinzl, F., Lorenz, S., Scholz-Kreisel, P., & Weiskopf, D. (2024). Filling data gaps in long-term solar UV monitoring by statistical imputation methods. *Photochemical & Photobiological Sciences*, *23*, 1265–1278. https://doi.org/10.1007/s43630-024-00593-8
49. World Meteorological Organization (WMO). Guide to instruments and methods of observation (WMO-No 8). Volume I–measurement of meteorological variables. Geneva, 2021–2025.
50. Hovila, J., Arola, A., & Tamminen, J. (2013). OMI/Aura surface UVB irradiance and erythemal dose daily L3 global gridded 1.0° x 1.0° V3. *NASA Goddard Space Flight Center Goddard Earth Sciences Data and Information Services Center (GES DISC) Dataset*. https://doi.org/10.5067/Aura/OMI/DATA3009
51. Kalakoski, N. (2016). OMI UVB level 3 (OMUVBd) product. Finnish meteorological institute. Retrieved April 18, 2026, from http://omi.fmi.fi/docs/OMUVB_L3d_Format_Specification_Document_v2_0.pdf
52. Ialongo, I., Casale, G. R., & Siani, A. M. (2008). Comparison of total ozone and erythemal UV data from OMI with ground-based measurements at Rome station. *Atmospheric Chemistry and Physics, 8*, 3283–3289. https://doi.org/10.5194/acp-8-3283-2008
53. Bernhard, G., Arola, A., Dahlback, A., Fioletov, V., Heikkilä, A., Johnsen, B., Koskela, T., Lakkala, K., Svendby, T., & Tamminen, J. (2015). Comparison of OMI UV observations with ground-based measurements at high northern latitudes. *Atmospheric Chemistry And Physics*, *15*, 7391–7412.
54. Zempila, M., Koukouli, M., Bais, A., Fountoulakis, I., Arola, A., Kouremeti, N., & Balis, D. (2016). OMI/Aura UV product validation using NILU-UV ground-based measurements in Thessaloniki, Greece. *Atmospheric Environment*, *140*, 283–297. https://doi.org/10.1016/j.atmosenv.2016.06.009
55. Mateos, D., Bilbao, J., Kudish, A. I., Parisi, A. V., Carbajal, G., di Sarra, A., Román, R., & de Miguel, A. (2013). Validation of OMI satellite erythemal daily dose retrievals using ground-based measurements from fourteen stations. *Remote Sensing of Environment, 128*, 1–10. https://doi.org/10.1016/j.rse.2012.09.009
56. Antón, M., Valenzuela, A., Román, R., Lyamani, H., Krotkov, N., Arola, A., Olmo, F. J., & Alados-Arboledas, L. (2012). Influence of desert dust intrusions on ground-based and satellite-derived ultraviolet irradiance in southeastern Spain. *Journal of Geophysical Research, 117*, Article D19209. https://doi.org/10.1029/2012JD018056
57. Bilbao, J., & de Migue, A. (2020). Erythemal solar irradiance, UVER, and UV index from ground-based data in central Spain. *Applied Sciences, 10*, Article 6589. https://doi.org/10.3390/app10186589
58. Kutal, G., Kolhe, A., Varpe, S., Mahajan, C., Singh, P., & Aher, G. (2022). UV erythemal radiation and its sensitivity to changes in total column ozone and aerosols. *Aerosol Science and Engineering, 6*, 176–185. https://doi.org/10.1007/s41810-022-00132-x
59. Lubitz, F., Dzwonek, A., Helletzgruber, S., Danhel, H., Radmanovic, D., Weihs, P., Kitz, E., & Schmalwieser, A. W. (2026). Methods for substituting ambient ultraviolet radiation exposure for personal exposure studies. *Photochemistry and Photobiology*. https://doi.org/10.1111/php.70108
60. Allaart, M., van Weele, M., Fortuin, P., & Kelder, H. (2004). An empirical model to predict the UV-index based on solar zenith angles and total ozone. *Meteorological Applications*, *11*, 59–65. https://doi.org/10.1017/S1350482703001130
61. Eskes, H. J., Van Velthoven, P. F. J., Valks, P. J. M., & Kelder, H. M. (2003). Assimilation of GOME total-ozone satellite observations in a three-dimensional tracer-transport model. *Quarterly Journal of the Royal Meteorological Society, 129*, 1663–1681. https://doi.org/10.1256/qj.02.14
62. Van Geffen, J., & van Weele, M. (2024). & van der A, R. UV index and UV dose: data product description, version 2.x. Royal Netherlands Meteorological Institute (KNMI)/TEMIS. Retrieved April 18, 2026, from https://www.temis.nl/uvradiation/product/
63. Zempila, M. M., Van Geffen, J. H. G. M., Taylor, M., Fountoulakis, I., Koukouli, M. E., Van Weele, M., Van der A, R. J., Bais, A., Meleti, C., & Balis, D. (2017). TEMIS UV product validation

using NILU-UV ground-based measurements in Thessaloniki, Greece. *Atmospheric Chemistry and Physics, 17*, 7157–7174. https://doi.org/10.5194/acp-17-7157-2017

64. Pfeifroth, U., Kothe, S., Drücke, J., Trentmann, J., Schröder, M., Selbach, N., & Hollmann, R. (2023). Surface Radiation Data Set - Heliosat (SARAH) - Edition 3. *Satellite Application Facility on Climate Monitoring*. https://doi.org/10.5676/EUM_SAF_CM/SARAH/V003
65. Pfeifroth, U., Drücke, J., Kothe, S., Trentmann, J., Schröder, M., & Hollmann, R. (2024). SARAH-3 – satellite-based climate data records of surface solar radiation. *Earth Syst Sci Data*, *16*, 5243–5265. https://doi.org/10.5194/essd-16-5243-2024
66. Müller, R., & Pfeifroth, U. (2022). Remote sensing of solar surface radiation – A reflection of concepts, applications and input data based on experience with the effective cloud albedo. *Atmospheric Measurement Techniques, 15*, 1537–1561. https://doi.org/10.5194/amt-15-1537-2022
67. Mueller, R., Behrendt, T., Hammer, A., & Kemper, A. (2012). A new algorithm for the satellite-based retrieval of solar surface irradiance in spectral bands. *Remote Sensing, 4*, 622–647. https://doi.org/10.3390/rs4030622
68. Karlsson, K. G., Riihelä, A., Trentmann, J., Stengel, M., Solodovnik, I., Meirink, J. F., Devasthale, A., Jääskeläinen, E., Kallio-Myers, V., Eliasson, S., Benas, N., Johansson, E., Stein, D., Finkensieper, S., Håkansson, N., Akkermans, T., Clerbaux, N., Selbach, N., Schröder, M., & Hollmann, R. (2023a). CLARA-A3: CM SAF cLoud, albedo and surface radiation dataset from AVHRR data-Edition 3. Satellite application facility on climate monitoring. https://doi.org/10.5676/EUM_SAF_CM/CLARA_AVHRR/V003
69. Mueller, R. W., Matsoukas, C., Gratzki, A., Behr, H. D., & Hollmann, R. (2009). The CM-SAF operational scheme for the satellite based retrieval of solar surface irradiance — A LUT based eigenvector hybrid approach. *Remote Sensing of Environment*, *113*, 1012–1024. https://doi.org/10.1016/j.rse.2009.01.012
70. Karlsson, K.-G., Stengel, M., Meirink, J. F., Riihelä, A., Trentmann, J., Akkermans, T., Stein, D., Devasthale, A., Eliasson, S., Johansson, E., Håkansson, N., Solodovnik, I., Benas, N., Clerbaux, N., Selbach, N., Schröder, M., & Hollmann, R. (2023b). CLARA-A3: The third edition of the AVHRR-based CM SAF climate data record on clouds, radiation and surface albedo covering the period 1979 to 2023. *Earth System Science Data, 15*, 4901–4926. https://doi.org/10.5194/essd-15-4901-2023
71. Ceppi, P., Wilson Kemsley, S., Andersen, H., Andrews, T., Kramer, R. J., Nowack, P., Wall, C. J., & Zelinka, M. D. (2026). Emerging low-cloud feedback and adjustment in global satellite observations. *Atmospheric Chemistry and Physics, 26*, 4153–4171. https://doi.org/10.5194/acp-26-4153-2026
72. Segado-Moreno, L. C., Ruiz-Arias, J. A., Montávez, J. P., & Betak, J. (2026). Past, current and future solar radiation trends in Europe: Multi-source assessment of the role of clouds and aerosols. *Remote Sensing of Environment, 333*, Article 115122. https://doi.org/10.1016/j.rse.2025.115122
73. Byrne, M. P., & O'Gorman, P. A. (2018). Trends in continental temperature and humidity directly linked to ocean warming. *Proceedings of the National Academy of Sciences of the United States of America, 115*(19), 4863–4868. https://doi.org/10.1073/pnas.1722312115
74. Liu, H., Koren, I., Altaratz, O., & Chekroun, M. D. (2023). Opposing trends of cloud coverage over land and ocean under global warming. *Atmospheric Chemistry And Physics*, *23*, 6559–6569. https://doi.org/10.5194/acp-23-6559-2023
75. Gröbner, J., Albold, A., Blumthaler, M., Cabot, T., De la Casiniere, A., Lenoble, J., Martin, T., Masserot, D., Müller, M., Philipona, R., Pichler, T., Pougatch, E., Rengarajan, G., Schmucki, D., Seckmeyer, G., Sergent, C., Touré, M. L., & Weihs, P. (2000). Variability of spectral solar ultraviolet irradiance in an Alpine environment. *Journal of Geophysical Research, 105*(D22), 26991–27003. https://doi.org/10.1029/2000JD900395
76. Fears, T. R., Scotto, J., & Schneidermann, M. A. (1977). Mathematical models of age and ultraviolet effects on the incidence of skin cancer among whites in the United States. *Am J Epidermiol*, *105*, 420–427.
77. Slaper, H., Schothorst, A. A., & Van Der Leun, J. C. (1986). Risk evaluation of UVB therapy for psoriasis: Comparison of calculated risk for UVB therapy and observed risk in PUVA-treated patients. *Photodermatology*, *3*, 271–283.
78. Diffey, B. L. (1987). Analysis of the risk of skin cancer from sunlight and solaria in subjects living in northern Europe. *Photodermatology*, *4*, 118–126.
79. Cabaj, A., Schauberger, G., & Keck, G. (1992). Nicht-melanomer Hautkrebs in Österreich: Vergleich von statistischen Daten mit Ergebnissen von Modellrechnungen. *Zeitschrift Fur Medizinische Physik*, *2*, 165–168. https://doi.org/10.1016/S0939-3889(15)70698-7
80. Vishvakarman, D., & Wong, J. C. F. (2003). Description of the use of a risk estimation model to assess the increased risk of non-melanoma skin cancer among outdoor workers in Central Queensland, Australia. *Photoderm Photoimmun Photomed*, *19*, 81–88.
81. German Commission on Radiological Protection. (2023). Dose-response relationship for the association of UV radiation and skin cancer-Statement by the German Commission on Radiological Protection. Strahlenschutzkommission. https://ssk.de/fileadmin/documents/de/2023/2023-02-03_Stg_Dosiswirkungsbeziehungen_UV.pdf

Authors and Affiliations

Alois W. Schmalwieser[1] · Sebastian Lorenz[2] · Dariia Klyshkina[1] · Barbara Klotz[3] · Michael Schwarzmann[3] · Stana Simic[4] · Alexander Mangold[5] · Natacha Pezzetti[5] · Kamil Láska[6] · Marie Novotná[6] · Martin Stráník[7] · Brian Køster[8] · Margit Aun[9] · Kaisa Lakkala[10,11] · Frederique Auriol[12] · Eric Bourrianne[12] · Romain De Filippi[12] · Nicolas Henriot[12] · Fanny Minvielle[12] · Jörg Trentmann[13] · Daniela Weiskopf[2] · Alkiviadis Bais[14] · Katerina Garane[14] · Dénes Fekete[15] · Annachiara Bellini[16] · Alcide Giorgio di Sarra[17] · Henri Diémoz[16] · Luca Fibbi[18,19] · Francesca Frasca[20] · Daniele Grifoni[18,19] · Daniela Meloni[17] · Anna Maria Siani[20] · Peter den Outer[21] · Jos van Geffen[22] · Edith van Putten[21] · Bjørn Johnsen[23] · Tove Svendby[24] · Agnieszka Czerwińska[25] · Janusz Krzyścin[25] · Natalia Chubarova[26] · Slavica Malinović-Milićević[27,28] · Zoltan Nađ[29] · Zorica Podrascanin[29] · Anna Pribullova[30] · Juana Arolo Pacheco[31] · Ana Díaz Rodriguez[31] · Carmen González[32] · José Manuel Vilaplana[32] · Julian Gröbner[33] · Gregor Hülsen[33] · Michael Higlett[34] · Andrey Lyachev[34] · Rebecca Rendell[34] · Andrew R. D. Smedley[35] · Ann Webb[35]

✉ Alois W. Schmalwieser
alois.schmalwieser@vetmeduni.ac.at

[1] Unit of Medical Physics and Biophysics, University of Veterinary Medicine, Vienna, Austria

[2] Federal Office for Radiation Protection, Oberschleissheim, Germany

[3] Institute of Biomedical Physics, Medical University Innsbruck, Innsbruck, Austria

[4] Institute of Meteorology and Climatology, BOKU University, Vienna, Austria

[5] Group Atmospheric Composition, Measurement and Modelling, ACM2, Royal Meteorological Institute of Belgium, Brussels, Belgium

[6] Department of Geography, Faculty of Science, Masaryk University, Brno, Czech Republic

[7] Solar and Ozone Department (SOO), Czech Hydrometeorological Institute (CHMI), Hradec Kralove, Czech Republic

[8] Danish Cancer Society, Copenhagen, Denmark

[9] Centre for Climate Research, Institute of Physics, University of Tartu, Tartu, Estonia

[10] Space and Earth Observation Centre, Finnish Meteorological Institute, Sodankylä, Finland

[11] Climate Research Programme, Finnish Meteorological Institute, Kuopio, Finland

[12] Laboratoire d'Optique Atmosphérique (LOA), Univ. de Lille/CNRS, Lille, France

[13] Satellitengestütztes Klimamonitoring, Deutsche Wetterdienst (DWD), Offenbach, Germany

[14] Laboratory of Atmospheric Physics, Aristotle University of Thessaloniki, Thessaloniki, Greece

[15] Hungarian Meteorological Service (HungaroMet), Budapest, Hungary

[16] Regional Environmental Protection Agency (ARPA) of the Aosta Valley, Saint-Christophe, Italy

[17] Sustainability Department, Italian National Agency for New Technologies, Energy, and Sustainable Economic Development (ENEA), Rome, Italy

[18] Institute of Bioeconomy (IBE), National Research Council (CNR), Sesto Fiorentino, Italy

[19] LaMMA Consortium , Sesto Fiorentino, Italy

[20] Physics Department, Sapienza University of Rome, Rome, Italy

[21] National Institute for Public Health and the Environment (RIVM), Bilthoven, The Netherlands

[22] Royal Netherlands Meteorological Institute (KNMI), De Bilt, The Netherlands

[23] Norwegian Radiation and Nuclear Safety Authority (DSA), Oesteraas, Norway

[24] The climate and environmental research institute NILU, Kjeller, Norway

[25] Institute of Geophysics, Polish Academy of Sciences, Warsaw, Poland

[26] Faculty of Geography, Lomonosov Moscow State University, Moscow, Russia

[27] Geographical Institute "Jovan Cvijić", Serbian Academy of Sciences and Arts, Belgrade, Serbia

[28] Institute of Environmental Engineering, Peoples' Friendship University of Russia, RUDN University, Moscow, Russian Federation

[29] Faculty of Sciences, Department of Physics, University of Novi Sad, Novi Sad, Serbia

[30] Aerological and radiation centrum, Slovak hydrometeorological institute, Ganovce, Poprad, Slovakia

[31] Special Netwoks and Atmosphere Watch Service, Spanish Meteorological Agency (AEMET), Madrid, Spain

[32] Área de Investigación e Instrumentación Atmosférica, Instituto Nacional de Técnica Aeroespacial (INTA), El Arenosillo, Huelva, Spain

[33] Physikalisch-Meteorologisches Observatorium Davos, World Radiation Center (PMOD/WRC), Davos Dorf, Switzerland

[34] UK Health Security Agency, Radiation, Chemicals, Climate and Environmental Hazards Directorate, Didcot, Chilton, UK

[35] Department of Earth and Environmental Sciences, University of Manchester, Manchester, UK